DEVELOPMENT OF FLOOD RISK MAPS USING AN INTEGRATED HYDRODYNAMIC MODEL AND FAHP IN THE LOWER NAM PHONG BASIN, THAILAND

Chalermchai PAWATTANA[1], Phaisarn JEEFOO [2*], Chaiwiwat VANSAROCHANA[3] & Satit POOPIWKHAM [4]

DOI: 10.21163/GT_2026.211.20

ABSTRACT

Flooding frequently affects rivers and low-lying areas of the Phong River, making flood risk assessment essential for mitigation and loss reduction. This study developed flood risk maps for the Lower Nam Phong basin using a fuzzy analytic hierarchy process (FAHP) integrated with GIS. Hazard (flood depth, slope, soil drainage) and vulnerability (land use) weights were derived through FAHP. Results show that under baseline conditions, 19.44% of Nong Bua, Bung Nium, and Khok Sri Sub-Districts were classified as high risk, consistent with historical flood records. Future scenarios indicate downstream expansion of high-risk zones: 10.45% under RCP 4.5 (Representative Concentration Pathways) and 12.00% under RCP 8.5, particularly in Bung Nium and Khok Sri. Across all scenarios, medium-risk areas dominated (8.13, 36.45, and 72.67 km^2 for baseline, RCP 4.5, and RCP 8.5, respectively). The maps provide actionable insights for flood management and planning in the basin.

Keywords: *Climate change; Representative Concentration Pathways (RCP); Flood risk; Fuzzy analytic hierarchy process (FAHP); GIS; Lower Nam Phong basin;*

1. INTRODUCTION

Floods are among Thailand's most destructive hazards (Singkran, 2017), repeatedly affecting the Lower Nam Phong basin (Nut et al., 2013). The 2011 flood, driven by extreme rainfall and tropical storms, caused widespread damage to agriculture, infrastructure, and livelihoods, highlighting the basin's vulnerability (Promchote et al., 2016). Despite this history, basin-specific flood risk maps that integrate physically based hydrodynamic modeling with transparent vulnerability weighting remain scarce. Previous studies often relied on single hazard indices or heuristic scoring, with limited validation against observed events, leaving a gap in reliable tools for local flood management (Arianti et al., 2023; Maranzoni et al., 2023; Bokhari et al., 2024).

Flood risk is commonly defined as the interaction of hazard and vulnerability (Vojinovic et al., 2016; Hagos et al., 2022; Edamo et al., 2023). Hazard factors such as flood depth, slope, and soil drainage determine physical exposure (Hu et al., 2017), while land use strongly influences socioeconomic vulnerability (Lai et al., 2015; Cikmaz et al., 2023).

[1]*Sustainable Infrastructure Research and Development Center, Department of Civil Engineering, Faculty of Engineering, Khon Kaen University, Thailand, chapaw@kku.ac.th (CP).*
[2*] *Geographic Information Science, School of Information and Communication Technology, University of Phayao, Thailand. Corresponding author phaisarn.je@up.ac.th (PJ).*
[3]*Department of Natural Resources and Environment, Faculty of Agriculture Natural Resources and Environment, Naresuan University, Thailand, chaiwiwatv@nu.ac.th (CV).*
[4]*Department of Highways, Khon Kaen 3 Ban Phai Highway District, Thailand, satit_tue@hotmail.co.th (SP).*

Multi-criteria decision-making methods, particularly the analytic hierarchy process (AHP), have been widely applied to flood risk assessment (Liu et al., 2020). However, conventional AHP struggles with uncertainty in expert judgment. The fuzzy analytic hierarchy process (FAHP) extends AHP by incorporating fuzzy numbers, improving robustness under subjective evaluations (Baalousha et al., 2023). Coupling FAHP with hydrodynamic simulation and GIS provides a systematic framework for spatial risk mapping (Ahmad et al., 2022; Cikmaz et al., 2023).

This study develops an integrated SWAT-MIKE-FAHP-GIS framework tailored to the Lower Nam Phong basin. Hydrologic and hydrodynamic models simulate flood depths under baseline and climate scenarios (RCP 4.5 and 8.5), while FAHP weights hazard and vulnerability indicators based on expert input. Validation combines satellite-derived inundation, historical flood records, and community insights. The research addresses three questions: (i) How do baseline and climate scenarios translate into flood depths and extents? (ii) How do FAHP-derived weights influence spatial risk patterns? (iii) What uncertainties affect interpretation and operational use? By answering these, the study contributes reproducible methods and actionable maps to support zoning, preparedness, and mitigation planning in a flood-prone Thai basin.

2. STUDY AREA

The Phong River basin in northeastern Thailand consists of two sub-basins: the Upper Nam Phong (12,253 km^2) and the Lower Nam Phong (2,937 km^2) (**Fig. 1**). The study focuses on the Lower Nam Phong, located between 16°30′0″ N to 17°30′0″ N and 102°0′0″ E to 103°0′0″ E, which has repeatedly experienced damaging floods, including the 2011 event. Average annual rainfall is 1,130 mm (1986-2018), with extreme 3-day totals ranging from 50 to 177 mm that have triggered inundation downstream.

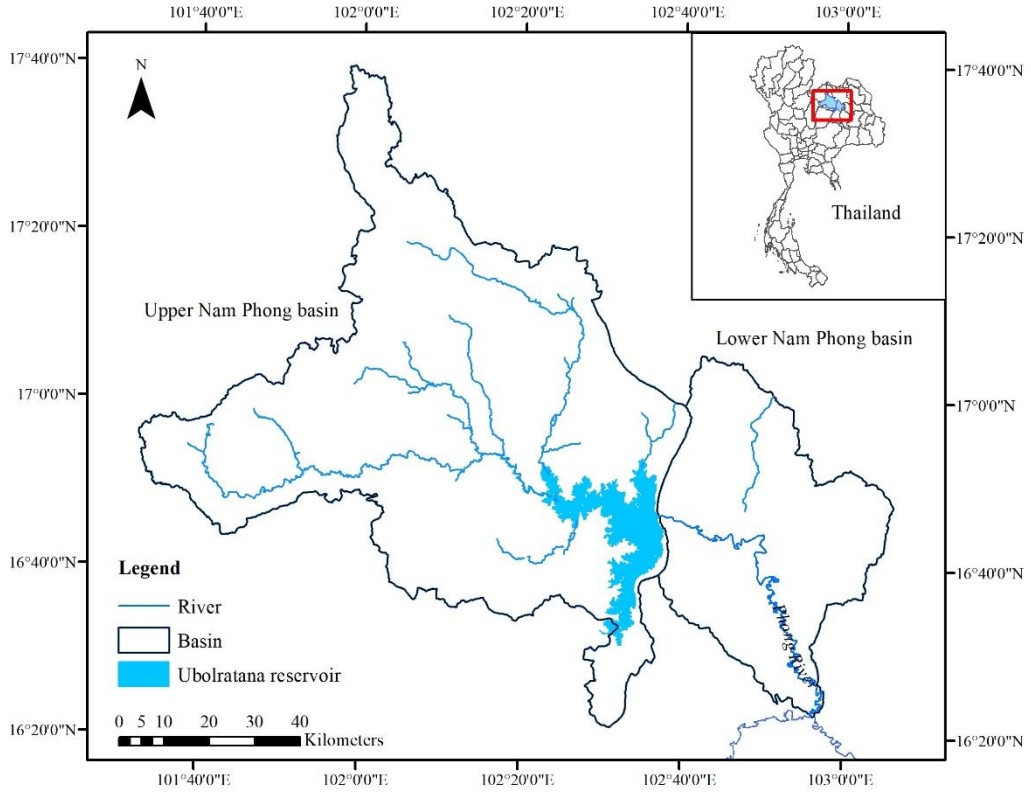

Fig. 1. Location map of the study area.

The Upper basin contains the Ubolratana Dam, with a storage capacity of 2,400 MCM and average inflow of 2,515 MCM (1986-2018), ranging from 567 to 5,425 MCM (Pawattana et al., 2021). Reservoir operations influence downstream hydrology, making the Lower basin particularly vulnerable to flood hazards. For this study, rainfall and temperature time series, a 30 m SRTM DEM (WGS84, Zone 48N), soil drainage and land-use data (the Land Development Department (LDD) of Thailand, 2016), and RADARSAT-1 imagery (21 September 2011) were compiled. All spatial datasets were harmonized to a 30 m grid for integration with hydrologic-hydrodynamic modeling and FAHP analysis. These inputs provide the basis for simulating flood depths and assessing risk under baseline and climate scenarios.

3. DATA AND METHODS

3.1. Fuzzy analytic hierarchy process

Flood risk assessment requires systematic weighting of hazard and vulnerability factors. Conventional AHP is widely used but limited in handling uncertainty in expert judgment (Hategekimana et al., 2018; Putra et al., 2018). FAHP extends AHP by incorporating triangular fuzzy numbers (TFNs), which better capture ambiguity in pairwise comparisons (Yang et al., 2013; Emrouznejad & Ho, 2018; Peng et al., 2021). In this study, six experts with backgrounds in hydrology, GIS, and disaster management provided judgments. Divergent opinions were averaged, and consistency was checked (CR < 0.1) to ensure reliability. The following are the processes of FAHP (Parsian et al., 2021; Yodying et al., 2022).

Table 1.

Fuzzy scale for pairwise comparison.

Definition	Crisp scale	Fuzzy scale
Equal importance	1	(1, 1, 1)
Somewhat more important	3	(2, 3, 4)
Much more important	5	(4, 5 ,6)
Very much more important	7	(6, 7, 8)
Absolutely more important	9	(8, 9, 9)
Intermediate values	2, 4, 6, 8	(x-1, x, x+1)

Step 1. Hierarchical structure development: The primary and secondary criteria are established in accordance with the overarching objectives.

Step 2. Calculation of the fuzzified pairwise comparison matrix: Eq. 1 contains the pairwise comparison, where M_{gij} (i = 1, 2, ..., n and j = 1, 2, ..., m) are TFNs (Yodying et al., 2022).

$$\left(M_{gi}^{j}\right)_{nxm} = \begin{bmatrix} M_{g1}^{1} & M_{g1}^{2} & \cdots & M_{g1}^{m} \\ M_{g2}^{1} & M_{g2}^{2} & \cdots & M_{g2}^{m} \\ \vdots & \vdots & & \vdots \\ M_{gn}^{1} & M_{gn}^{2} & \cdots & M_{gn}^{m} \end{bmatrix} = \begin{bmatrix} (1,1,1) & \left(l_{1_2}, m_{1_2}, u_{1_2}\right) & \cdots & \left(l_{1_m}, m_{1_m}, u_{1_m}\right) \\ \left(l_{2_1}, m_{2_1}, u_{2_1}\right) & (1,1,1) & \cdots & \left(l_{2_m}, m_{2_m}, u_{2_m}\right) \\ \vdots & \vdots & \vdots & \vdots \\ \left(\frac{1}{u_{n_1}}, \frac{1}{m_{n_1}}, \frac{1}{l_{n_1}}\right) & \left(\frac{1}{u_{n_2}}, \frac{1}{m_{n_2}}, \frac{1}{l_{n_2}}\right) & \cdots & (1,1,1) \end{bmatrix} \quad (1)$$

Step 3: Calculation of the imprecise synthetic extent: This phase is computed using Eq. 2.

$$S_i = \sum_{j=1}^{m} M_{gi}^{j} \times \left[\sum_{i=1}^{n} \sum_{j=1}^{m} M_{gi}^{j} \right] \tag{2}$$

where S_i is the synthetic extent value of the pairwise comparison and $\sum_{j=1}^{m} M_{gi}^{j}$ is the total number of TFNs. Additional information is provided in Eqs. 3 to 5, correspondingly.

$$\sum_{j=1}^{m} M_{gi}^{j} = \left[\sum_{j=1}^{m} l_j, \sum_{j=1}^{m} m_j, \sum_{j=1}^{m} u_j \right] \tag{3}$$

$$\sum_{i=1}^{n} \sum_{j=1}^{m} M_{gi}^{j} = \left(\sum_{i=1}^{n} l_i, \sum_{i=1}^{n} m_i \sum_{i=1}^{n} u_i \right) \tag{4}$$

$$\left[\sum_{i=1}^{n} \sum_{j=1}^{m} M_{g}^{j} \right]^{-1} = \left(\frac{1}{\sum_{i=1}^{n} l_i}, \frac{1}{\sum_{i=1}^{n} m_i}, \frac{1}{\sum_{i=1}^{n} u_i} \right) \tag{5}$$

Step 4. Utilize the equation below to determine the degree of probability.

$$V\left(S_i \geq S_j\right) = \begin{cases} 1 & m_i \geq m_j \\ 0 & if \quad l_j \geq u_i \\ \dfrac{l_j - u_i}{\left(m_i - u_i\right) - \left(m_j - l_j\right)} & otherwise \end{cases} \tag{6}$$

In the case of S_i is greater than S_j, then $V\left(S_i \geq S_j \,|\, j = 1, 2, ..., m; \neq j\right) = \min V\left(S_i \geq S_j \mid j = 1, 2, ..., m; \neq j\right)$.

Step 5. Determine the weight vector: The definition of a weight vector is as follows:

$$W_i^{'} = \min V\left(S_i \geq S_j \,|\, j = 1, 2, ..., i \neq j\right) \tag{7}$$

$$W_i = \frac{w_i^{'}}{\sum_{i=1}^{n} w_i^{'}} \tag{8}$$

where the term W, is defined as $(w_1, w_2, ..., w_n)^{\mathrm{T}}$, is a weight vector that has been normalized. The non-fuzzy number (w_i) for each weight will be derived then.

Step 6. Consistency determination: The comparison matrix is established by the consistency of the evaluation, as indicated by the expert decision. Eq. 9 is applied to calculate the consistency index (*CI*), which is used to determine the degree of consistency.

$$CI = \frac{\lambda_{\max} - n}{n - 1} \tag{9}$$

where λ_{max} and n are the maximum eigenvector derived from the calculation of pairwise comparison matrix and the number of factors. The consistency ratio (CR) is computed using Eq. 10 to certify the acceptance of the degree of consistency.

$$CR = \frac{CI}{RI} \tag{10}$$

where RI is the random inconsistency which depends on the number of factors. The consistency of the judgment matrix is satisfactory, as indicated by $CR < 0.1$. The consistency of the judgment matrix must be reevaluated when CR is greater than or equal to 0.1 (Peng et al., 2021).

3.2. Evaluation of flood risk

Flood risk was defined as the product of hazard and vulnerability (Risk = Hazard × Vulnerability) (Vojinovic et al., 2016). Hazard scores were derived from hydrologic-hydrodynamic simulations of flood depth, slope, and soil drainage, while vulnerability scores were based on land use. FAHP weights were applied to each factor, and risk scores were computed in GIS. Raster layers (30 m resolution) were classified into low, medium, and high risk using the standard deviation method, chosen for its suitability in continuous hazard data and comparability across scenarios. Referring **Fig. 2**, the flowchart depicts the processes to derive the flood risk maps using FAHP and GIS database.

Furthermore, flood risk scores (*FRS*) are generated by multiplying the flood hazard score (*FHS*) and flood vulnerability score (*FVS*) (Eq. 11).

$$FRS = FHS \times FVS \tag{11}$$

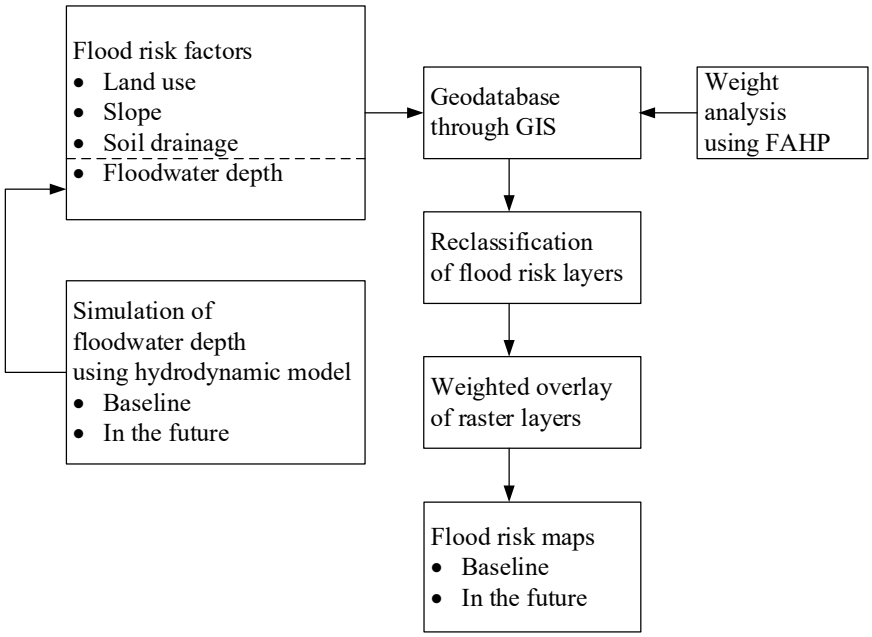

Fig. 2. Work flow of flood risk map development.

The flood hazard score is calculated by

$$FHS = wm_{Fd} \times wsub_{Fd} + wm_{Sl} \times wsub_{Sl} + wm_{Sd} \times wsub_{Sd} \quad (12)$$

where wm_{Fd}, wm_{Sl}, and wm_{Sd} are the weights of main-criteria for floodwater depth, slope, and soil drainage, respectively. $wsub_{Fd}$, $wsub_{Sl,}$ $wsub_{Sd}$ indicate the weights of each. The score of vulnerability is computed from Eq. 13.

$$FVS = wm_{Lu} \times wsub_{Lu} \quad (13)$$

where wm_{Lu} and $wsub_{Lu}$ stand for the weights of main and sub-criteria for land use.

Then, the weight values were input into the risk factors through GIS database. According to the utilization of Eqs. 12 and 13 to compute *FHS* and *FVS* and the process of reclassification, the risk layers in the vector format were converted into the raster format with the resolution of 30x30 m^2. Finally, the weighted overlay of raster layer using Eq. 11 was employed to calculate *FRS* and classified by the standard deviation method into low-, medium-, and high-level to derive the flood risk maps (Gigovic' et al., 2017).

3.3. Flood risk factors

3.3.1. Slope

The digital elevation data of the NASA Shuttle Radar Topographic Mission (SRTM) from USGS EarthExplorer (https://earthexplorer.usgs.gov/) has provided the digital elevation model (DEM) with resolution of 30x30 m^2. Positions of elevation data are a WGS84 horizontal datum with zone 48 N. The selection of 54 references elevation data was used to test the accuracy of DEM with R-square value of 0.78. The slope was generated directly from the DEM data by ArcGIS version 10.8 software and classified into five levels such as 0-5%, 5-12%, 12-20%, 20-35%, and more than 35%, respectively (**Fig. 3 (a)**).

3.3.2. Soil drainage

The sort of soil particle characteristics of year 2005 present in this study is indicated in **Fig. 3 (b)**, which has significant impact on the likelihood of flooding. The information was gathered from the LDD of Thailand. According to soil series and performance of permeability existing in the original GIS database, soil drainage layer was reclassified as very poor drainage, poor drainage, moderate drainage, good drainage, and very good drainage (Poopiwkham, 2018).

3.3.3. Land use

The different types of land use of year 2016 was collected from the LDD of Thailand. Many kinds of land use were classified into agriculture, forest, urban, and village (**Fig. 3 (c)**) (Poopiwkham, 2018; Hussain et al., 2021). The agricultural area consists of mostly irrigated rice areas and rainfed rice fields. The forest area comprises dry evergreen forest, mixed forest, and forest plantation. Urban area contains city and commercial areas, government office, and industrial areas. Village area comprises rural villages rely on their homes. Water body consists of water sources and natural water sources.

3.3.4. Floodwater depth

Simulated using hydrodynamic models for baseline (1989-2018) and future scenarios (2020-2049). The 3-day 50-year rainfall was derived from frequency analysis of annual maxima (1989-2018). Future rainfall inputs (RCP 4.5 and 8.5) were obtained from CNRM-CM5 projections downscaled via CORDEX and bias-corrected using quantile mapping (Anuthaman et al., 2023; Satriagasa et al., 2023). RCP 4.5 represents moderate stabilization, while RCP 8.5 reflects high-emission futures, bracketing plausible climate impacts. MIKE-11 was applied to simulate 1D unsteady flow along the Phong River, while MIKE-21 modeled 2D floodplain inundation. These outputs provided flood depth, velocity, and extent for risk assessment.

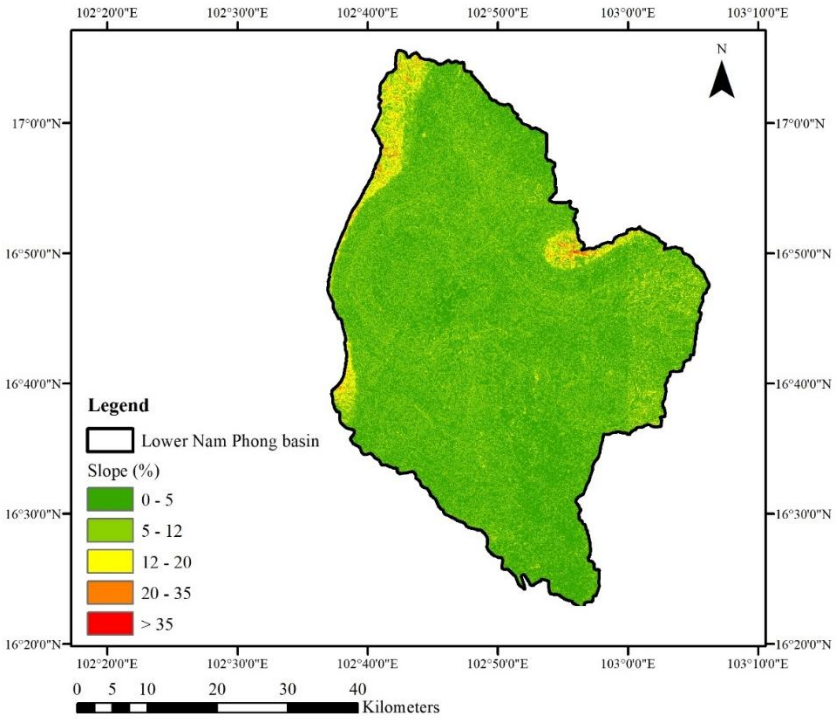

Fig. 3 (a) Slope.

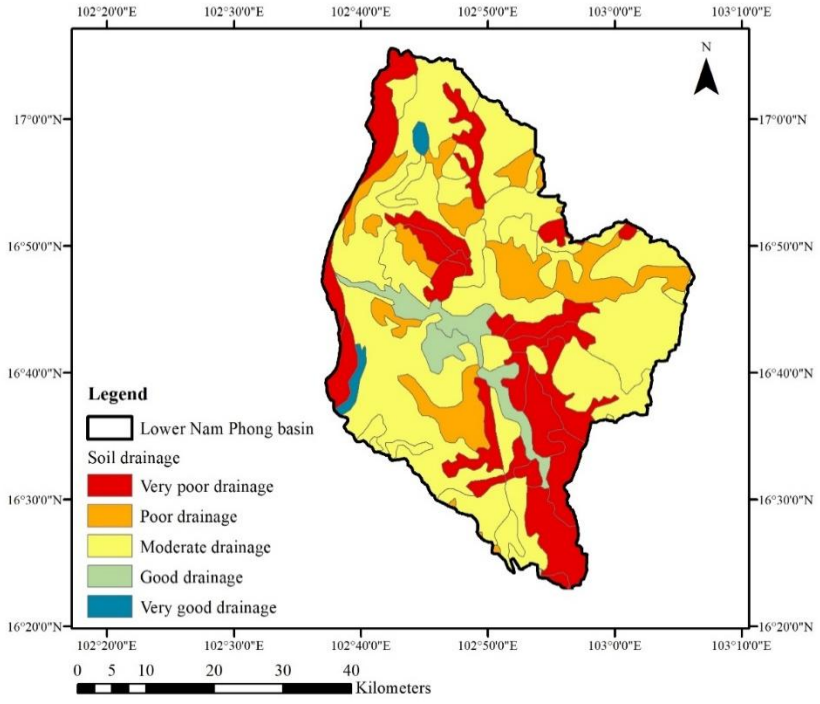

Fig. 3 (b) Soil drainage.

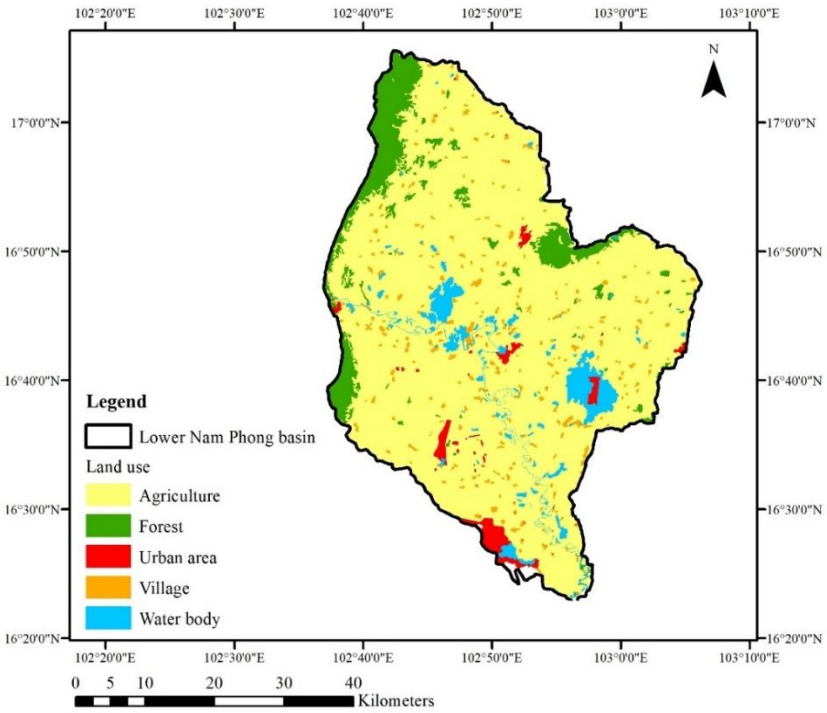

Fig. 3 (c) Land use.

Fig. 3. Maps of slope, soil drainage, and land use.

3.4. Hydrologic and Hydrodynamic Models

The Soil and Water Assessment Tool (SWAT) model was used to simulate runoff and lateral inflows (Li & Fang, 2021; M′Barek et al., 2021). Sub-basins and hydrologic response units (HRUs) were delineated using DEM, soil, and land-use inputs. Runoff was calculated using the SCS-CN method, infiltration by Green–Ampt, and streamflow calibrated (2005-2011) and validated (2012-2014) with NSE and R^2 metrics.

MIKE-11 simulated 1D unsteady flow along the Phong River using Saint-Venant equations, with Manning's n = 0.025-0.040 for channels and floodplains. MIKE-21 modeled 2D floodplain routing and inundation, including the 21 September 2011 flood event. Mesh resolution and stability were checked, and inundation extents compared with RADARSAT-1 imagery (76% overlap), confirming model reliability.

3.5. Performance and Uncertainty

Model performance was evaluated using R^2 and Nash‑Sutcliffe Efficiency (NSE), both yielding satisfactory values for calibration and validation (Parhi et al., 2012; Swagatika et al., 2022). Uncertainty arises from parameter sensitivity, input data accuracy, expert judgment variability, and climate projection assumptions. These limitations were acknowledged, and future work will incorporate probabilistic inundation modeling, expanded hazard indicators, and broader stakeholder engagement to strengthen robustness. The two indices are expressed mathematically in the following Eqs. 14 and 15, respectively.

$$R^2 = \left[\frac{\sum_{i=1}^{n} \left(y_i^{obs} - y_{mean}^{obs} \right) \left(y_i^{sim} - y_{mean}^{sim} \right)}{\sqrt{\sum_{i=1}^{n} \left(y_i^{obs} - y_{mean}^{obs} \right)^2} \sqrt{\sum_{i=1}^{n} \left(y_i^{sim} - y_{mean}^{sim} \right)^2}} \right]^2 \quad (14)$$

$$NSE = 1 - \left[\frac{\sum_{i=1}^{n} \left(y_i^{obs} - y_i^{sim} \right)^2}{\sum_{i=1}^{n} \left(y_i^{obs} - y_{mean}^{obs} \right)^2} \right] \quad (15)$$

where, y_i^{obs} and y_i^{sim} are the ith observed and simulated data. y_{mean}^{obs} and y_{mean}^{sim} are the mean observed and simulated data, and n is the total number of observations.

4. RESULTS AND DISCUSSIONS

4.1. Flood depth simulation

The SWAT model successfully simulated lateral inflows to the Phong River for both baseline (1989–2018) and future scenarios (2020-2049). Calibration (2005-2011) achieved NSE = 0.68 and R^2 = 0.70, while validation (2012-2014) yielded NSE = 0.79 and R^2 = 0.81, indicating satisfactory performance. These inflows were used as boundary conditions for MIKE hydrodynamic models.

MIKE-11 reproduced 1D unsteady flow with NSE and R^2 values above 0.75, while MIKE-21 simulated 2D floodplain inundation. Comparison with RADARSAT-1 imagery (21 September 2011) showed 76% spatial overlap, confirming credible hazard representation. The maximum 3-day rainfall of 177 mm (August 1991) produced 10.7 km^2 inundation under baseline conditions. Future scenarios projected 387 mm (RCP 4.5) and 468 mm (RCP 8.5), resulting in 43.35 km^2 and 89.05 km^2 inundation, respectively.

4.2. Weight analysis

FAHP weighting emphasized land use as the dominant vulnerability factor, reflecting the economic importance of irrigated rice fields. Hierarchical structure of flood risk depending on hazard and vulnerability is illustrated in **Fig. 4**.

Flood depth >2.75 m received the highest hazard weight, consistent with severe crop losses. Slope (0–5% irrigated, 5–12% rainfed) and poor soil drainage further increased vulnerability. Six experts contributed to pairwise comparisons; consistency ratios (CR < 0.1) confirmed reliability.

The **Table 2** shows the pairwise comparisons among the four main criteria (floodwater depth, slope, soil drainage, and land use). Land use received the highest weight, reflecting its dominant role in vulnerability. Consistency ratio (CR = 0.063) indicates reliable judgments.

The matrix (**Table 3**) presents expert comparisons of five soil drainage classes, from very poor to very good. Poorly drained soils were weighted highest, consistent with their strong influence on flood hazard. CR = 0.070 confirms acceptable consistency.

Slope categories (0-5%, 5-12%, 12-20%, 20-35%, >35%) were compared (**Table 4**). Gentle slopes (0-5%) received the highest weight, reflecting their greater susceptibility to inundation. CR = 0.077 indicates satisfactory consistency.

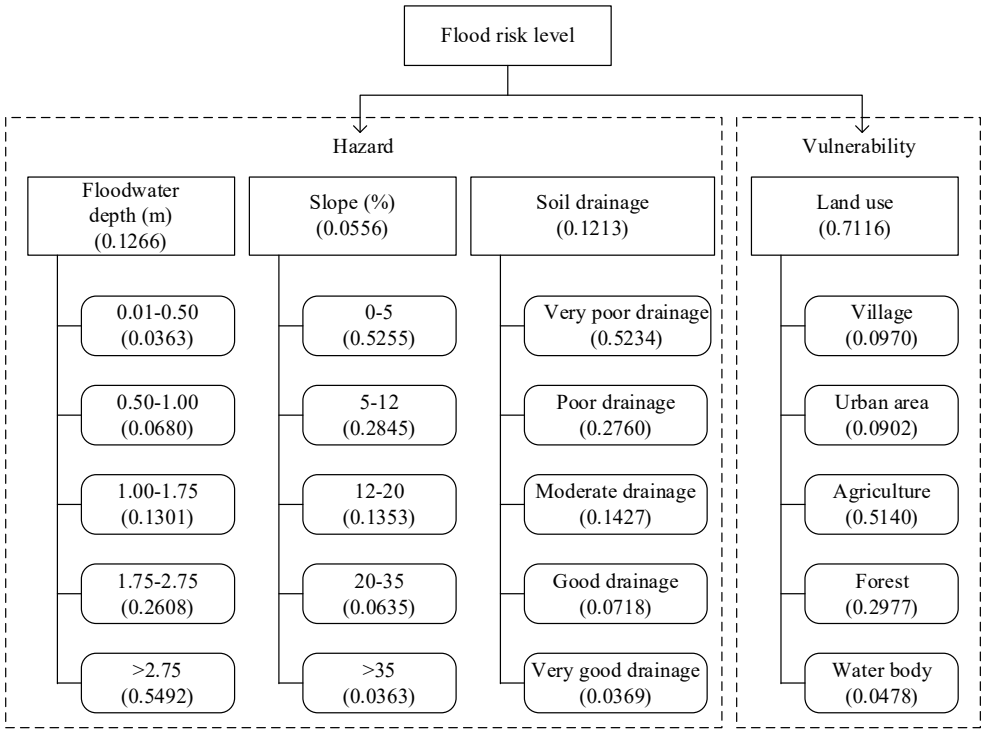

Fig. 4. Hierarchical structure of flood risk in Lower Nam Phong basin.

Table 2.

Main-criteria judgment matrix.

Main-criteria	Floodwater depth	Slope	Soil drainage	Land use
Floodwater depth	1,1,1	2,3,4	1,1,1	1/8,1/7,1/6
Slope	1/4,1/3,1/2	1,1,1	1/4,1/3,1/2	1/9,1/9/1/8
Soil drainage	1,1,1	2,3,4	1,1,1	1/9,1/9/1/8
Land use	6,7,8	8,9,9	8,9,9	1,1,1
λ_{max} = 4.17, *CI* = 0.056, *RI* = 0.89, *CR* = 0.063				

Table 3.

Sub-criteria judgment matrix of soil drainage.

Sub-criteria of soil drainage	Very poor drainage	Poor drainage	Moderate drainage	Good drainage	Very good drainage
Very poor drainage	1,1,1	2,3,4	4,5,6	6,7,8	8,9,9
Poor drainage	1/4,1/3,1/2	1,1,1	2,3,4	4,5,6	6,7,8
Moderate drainage	1/6,1/5,1/4	1/4,1/3,1/2	1,1,1	2,3,4	4,5,6
Good drainage	1/8,1/7,1/6	1/6,1/5,1/4	1/4,1/3,1/2	1,1,1	2,3,4
Very good drainage	1/9,1/9,1/8	1/8,1/7,1/6	1/6,1/5,1/4	1/4,1/3,1/2	1,1,1
λ_{max} = 5.31, CI = 0.078, RI = 1.11, CR = 0.070					

Table 4.

Sub-criteria judgment matrix of slope.

Sub-criteria of slope	0-5%	5-12%	12-20%	20-35%	>35%
0-5%	1,1,1	2,3,4	4,5,6	8,9,9	8,9,9
5-12%	1/4,1/3,1/2	1,1,1	2,3,4	6,7,8	6,7,8
12-20%	1/6,1/5,1/4	1/4,1/3,1/2	1,1,1	2,3,4	4,5,6
20-35%	1/9,1/9,1/8	1/8,1/7,1/6	1/4,1/3,1/2	1,1,1	2,3,4
>35%	1/9,1/9,1/8	1/8,1/7,1/6	1/6,1/5,1/4	1/4,1/3,1/2	1,1,1
λ_{max} = 5.34, *CI* = 0.086, *RI* = 1.11, *CR* = 0.077					

Table 5.

Sub-criteria judgment matrix of floodwater depth.

Sub-criteria of floodwater depth	0.01-0.50 m	0.50-1.00 m	1.00-1.75 m	1.75-2.75 m	>2.75 m
0.01-0.50 m	1,1,1	1/4,1/3,1/2	1/6,1/5,1/4	1/8,1/7,1/6	1/9,1/9,1/8
0.50-1.00 m	2,3,4	1,1,1	1/4,1/3,1/2	1/6,1/5,1/4	1/9,1/8,1/7
1.00-1.75 m	4,5,6	2,3,4	1,1,1	1/4,1/3,1/2	1/8,1/7,1/6
1.75-2.75 m	6,7,8	4,5,6	2,3,4	1,1,1	1/4,1/3,1/2
>2.75 m	8,9,9	7,8,9	6,7,8	2,3,4	1,1,1
λ_{max} = 5.35, *CI* = 0.089, *RI* = 1.11, *CR* = 0.080					

Flood depth ranges (0.01-0.50 m to >2.75 m) were evaluated. Depths exceeding 2.75 m obtained the highest weight, consistent with severe crop losses. CR = 0.080 demonstrates reliable expert agreement (**Table 5**).

Table 6.

Sub-criteria judgment matrix of land use.

Sub-criteria of land use	Village	Urban area	Agriculture	Forest	Water body
Village	1,1,1	1,1,1	1/6,1/5,1/4	1/6,1/5,1/4	2,3,4
Urban area	1,1,1	1,1,1	1/8,1/7,1/6	1/6,1/5,1/4	2,3,4
Agriculture	4,5,6	6,7,8	1,1,1	2,3,4	6,7,8
Forest	4,5,6	4,5,6	1/4,1/3,1/2	1,1,1	4,5,6
Water body	1/4,1/3,1/2	1/4,1/3,1/2	1/8,1/7,1/6	1/6,1/5,1/4	1,1,1
λ_{max} = 5.34, *CI* = 0.084, *RI* = 1.11, *CR* = 0.076					

Land use types (village, urban, agriculture, forest, water body) were compared (**Table 6**). Agriculture was assigned the highest weight due to its economic importance and vulnerability to flooding. CR = 0.076 confirms consistency of expert judgments.

4.3. Flood risk assessment

Risk maps (**Figs. 5-7**) classified areas into low, medium, and high risk using the standard deviation method. **Table 7** summarizes scenario differences:

- Baseline (1991 event): 19.44% high risk, concentrated in Nong Bua, Bung Nium, and Khok Sri.
- RCP 4.5: High risk reduced to 10.45%, but medium risk expanded to 36.45 km^2, covering downstream and midstream zones.
- RCP 8.5: High risk increased to 12.00%, with medium risk dominating (72.67 km^2), particularly in Bung Nium, Khok Sri, and Tha Kraserm.

This comparative presentation highlights the downstream expansion of risk under climate change, with irrigated rice fields consistently most vulnerable.

Fig. 5 presents flood risk map of the Lower Nam Phong basin for the baseline (1991 event). High-risk zones (19.44%) are concentrated in Nong Bua, Bung Nium, and Khok Sri, while medium-risk areas (76.98%) dominate across downstream and midstream sub-districts. Low-risk zones (3.58%) are scattered in Nong Bua, Khu Thong, Bung Nium, Khok Sri, Si La, and Muang Yarn.

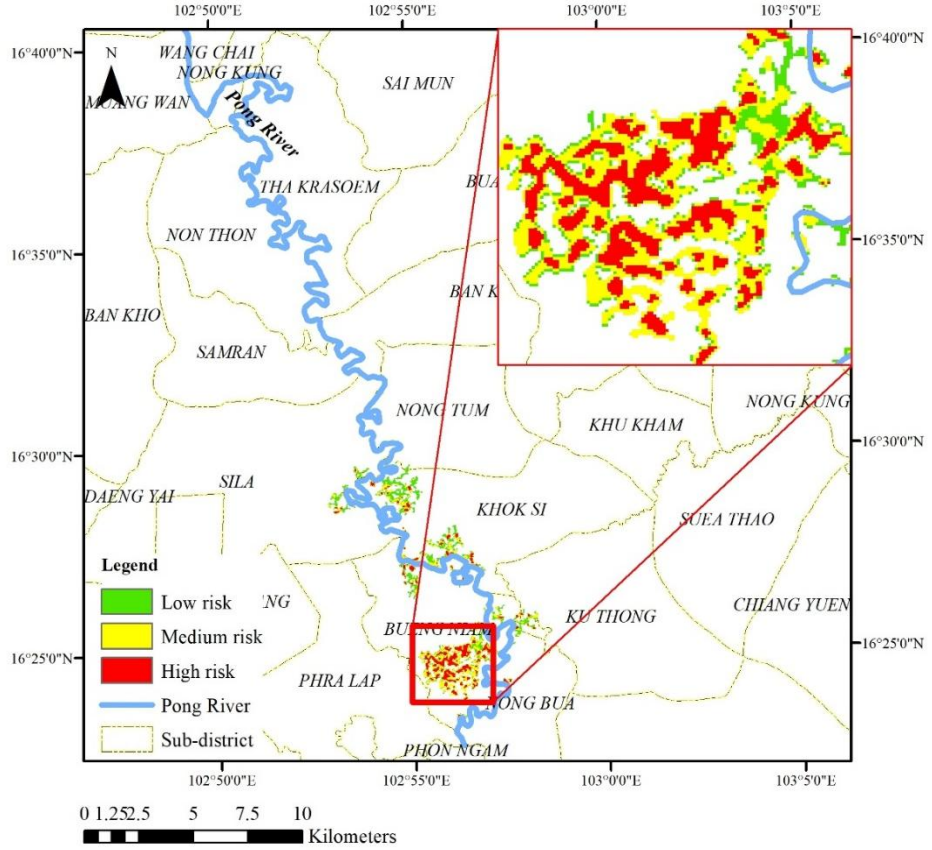

Fig. 5. Flood risk map of the Lower Nam Phong basin for baseline.

Fig. 6 presents flood risk map of the Lower Nam Phong basin under RCP 4.5 scenario (2020-2049). High-risk zones decrease to 10.45%, mainly in downstream areas (Nong Bua, Bung Nium, Pra Lab, Khu Thong, Khok Sri). Medium-risk zones expand to 36.45 km^2 (84.08%), covering downstream, midstream, and parts of upstream. Low-risk zones (5.47%) are distributed across Khok Sri, Si La, Non Thon, Tha Kraserm, Bung Nium, and Sai Mun.

Fig. 7 illustrates flood risk map of the Lower Nam Phong basin under RCP 8.5 scenario (2020-2049). High-risk zones increase to 12.00%, concentrated in Bung Nium and Khok Sri. Medium-risk zones dominate (72.67 km^2, 81.61%), particularly in Bung Nium, Khok Sri, Si La, Non Thon, and Tha Kraserm. Low-risk zones (6.39%) are scattered in Khok Sri, Si La, Non Thon, Tha Kraserm, and Ban Kham.

Table 7 illustrates areas (km^2) of flood risk levels under baseline and future scenarios. This table compares the extent of low-risk, medium-risk, and high-risk zones across baseline (1991 event), RCP 4.5, and RCP 8.5 scenarios. Results show that medium-risk areas expand substantially under climate change (36.45 km^2 in RCP 4.5 and 72.67 km^2 in RCP 8.5), while high-risk zones decrease under RCP 4.5 (4.53 km^2) but increase again under RCP 8.5 (11.57 km^2). The comparative values highlight the downstream expansion of flood risk and the growing vulnerability of agricultural land under future climate conditions.

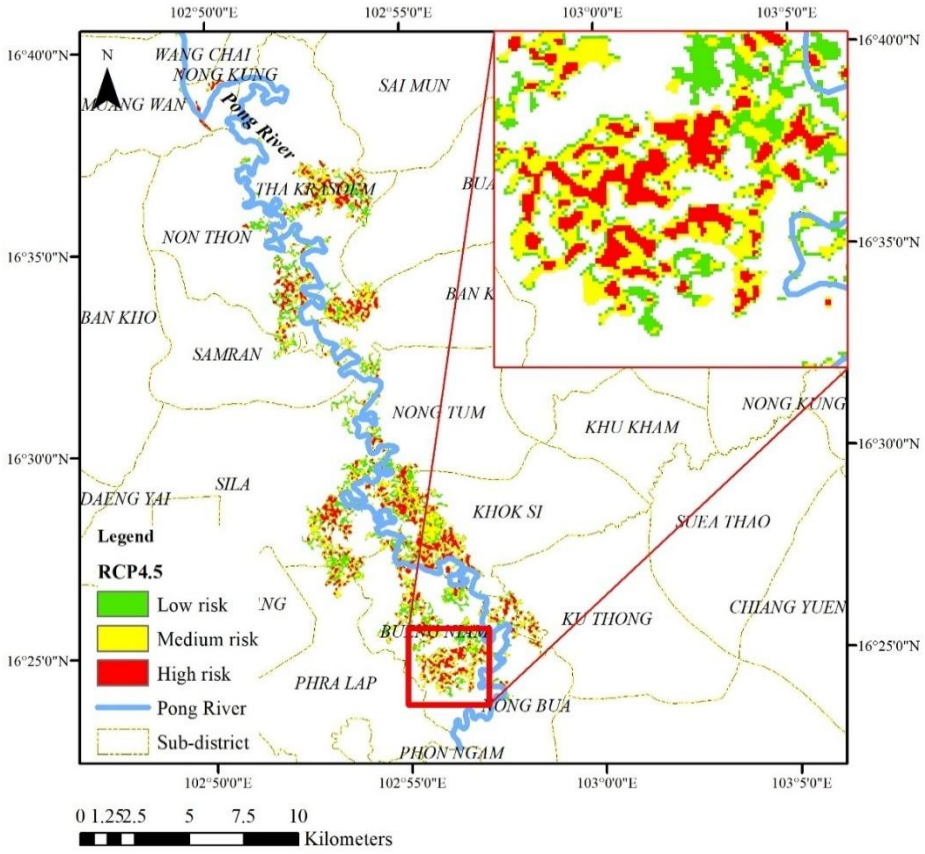

Fig. 6. Flood risk map of the Lower Nam Phong basin for RCP 4.5.

Table 7.
Areas (km^2) of various risk levels in the Lower Nam Phong basin.

Risk level / Scenario	Low-risk	Medium-risk	High-risk
Baseline	0.49	8.13	2.08
RCP 4.5	2.37	36.45	4.53
RCP 8.5	4.82	72.67	11.57

4.4. Validation of flood risk map

Validation combined multiple approaches:

- Historical comparison: High-risk zones matched flood events in 2011, 2017, and 2022 (Typhoon Noru).
- Community insights: Interviews confirmed prolonged inundation in rice fields, supporting land use weighting.
- Satellite overlap: 76% agreement between MIKE-21 outputs and RADARSAT-1 imagery.
- Model performance: NSE and R^2 values exceeded 0.75, supporting robustness.

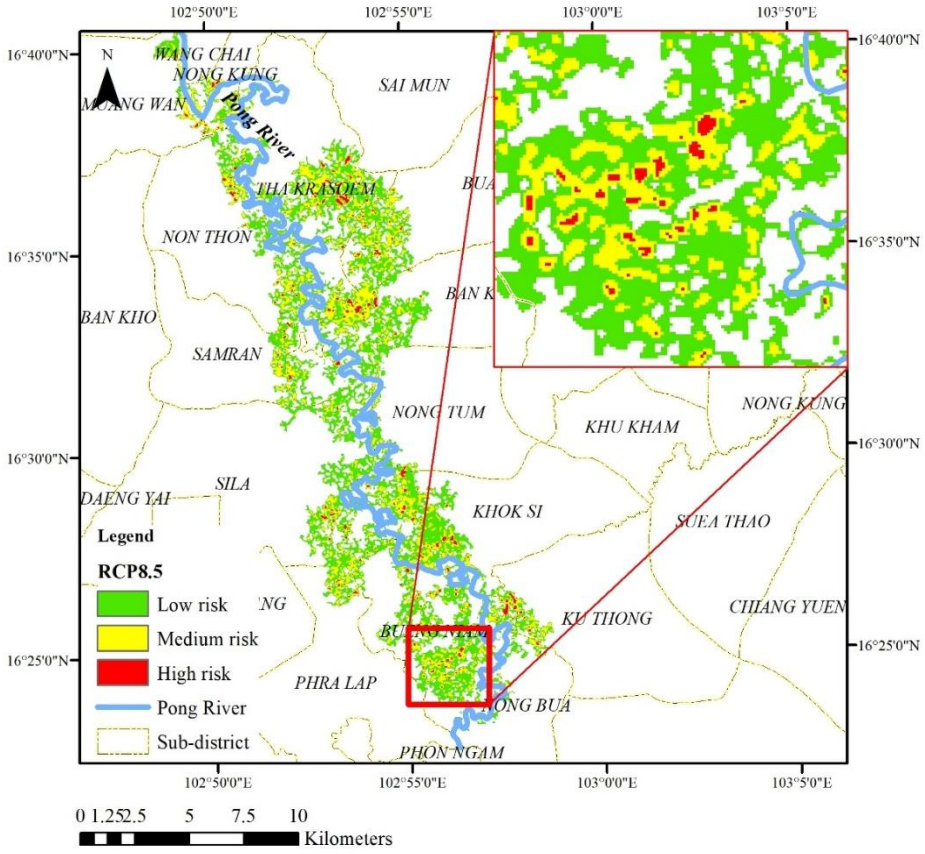

Fig. 7. Flood risk map of the Lower Nam Phong basin for RCP 8.5.

4.5. Uncertainty and Practical Relevance

Uncertainty arises from hydrodynamic parameters, expert judgment variability, limited flood events, and climate projection assumptions. While FAHP improves handling of subjective input, averaging expert scores may introduce bias. Future work should incorporate sensitivity analysis, probabilistic inundation modeling, and expanded datasets.

Practically, the maps provide actionable guidance for zoning, prioritizing structural and non-structural measures, and agricultural planning. The methodology is transferable to other flood-prone basins, offering a reproducible framework for climate-informed risk management.

5. CONCLUSIONS

This study developed and validated an integrated SWAT‑MIKE‑FAHP‑GIS framework for climate-informed flood risk mapping in the Lower Nam Phong basin. Validation against satellite imagery and historical floods confirmed credible hazard representation, while FAHP weighting highlighted land use particularly irrigated rice fields as the dominant vulnerability factor. Risk maps revealed medium risk zones across much of the basin, with high-risk areas clustering downstream and expanding under RCP 8.5, underscoring the influence of climate change on future flood exposure.

Key limitations include parameter and projection uncertainties, reliance on six expert judgments, and restricted flood event samples. The use of standard deviation for classification, while suitable for continuous hazard data, may yield different spatial outcomes under alternative schemes. Future work should incorporate additional hazard and vulnerability indicators, higher-resolution datasets, probabilistic inundation modeling, and broader stakeholder engagement. Explicit treatment of climate projection uncertainty and sensitivity analysis of hydrodynamic parameters would further strengthen robustness.

The developed maps provide a practical foundation for flood management, supporting zoning, prioritization of structural and non-structural measures, and agricultural planning. Beyond the Lower Nam Phong basin, the methodology is transferable to other flood prone basins where integrated hydrodynamic modeling and FAHP can enhance decision-making under uncertainty. Real-world implementation will require institutional readiness, long-term monitoring, and sustained collaboration among local authorities, communities, and researchers. Overall, the framework offers a replicable approach for climate-informed flood risk management.

ACKNOWLEDGEMENTS

Authors would like to acknowledge Department of Civil Engineering, Faculty of Engineering, Khon Kaen University for supporting the research budget. We would like to deliver special thanks to Nongwai Irrigation Project and Ubonratana dam for providing essential data.

REFERENCES

Ahmad, I., Wang, X., Waseem, M., Zaman, M., Aziz, F., Khan, R.Z.N. & Ashraf, M. (2022) Flood management, characterization and vulnerability analysis using an integrated RS-GIS and 2D hydrodynamic modelling approach: The case of Deg Nullah, Pakistan. *Remote Sensing,* 14 (2138), 1-19. https://doi.org/10.3390/rs14092138.

Anuthaman, S.N., Ramasamy, S., Ramasubbu, B. & Lakshminarayanan, B. (2023) Modelling and forecasting of urban flood under changing climate and land use land cover. *Journal of Water and Climate Change,* 14 (12), 4314-4335. http://dx.doi.org/10.2166/wcc.2023.164.

Arianti, I., Rafani, M., Fitriani, N. & Nizar. (2023) Spatial modeling of flood vulnerability as basic data for flood mitigation. *Civil Engineering Journal,* 9 (4), 787-798. https://doi.org/10.28991/CEJ-2023-09-04-02.

Baalousha, H.M., Younes, A., Yassin, M.A. & Fahs, M. (2023) Comparison of the fuzzy analytic hierarchy process (F-AHP) and fuzzy logic for flood exposure risk assessment in arid regions. Hydrology. 10(136), 1-22. https://doi.org/10.3390/hydrology10070136.

Bokhari, B.F., Tawabini, B. & Baalousha, H.M. (2024) A fuzzy analytical hierarchy process ‑GIS approach to flood susceptibility mapping in Neom, Saudi Arabia. *Frontiers in Water,* 6 (1388003), 1-14. https://doi.org/10.3389/frwa.2024.1388003 .

Cikmaz, B.A., Yildirim, E. & Demir, I. (2023) Flood susceptibility mapping using fuzzy analytical hierarchy process for Cedar Rapids, Iowa. *International Journal of River Basin Management*, 23, 1-13. https://doi.org/10.1080/15715124.2023.2216936.

Edamo, M.L., Hatiye, S.D. & Minda, T.T. (2023) Flood inundation and risk mapping under climate change scenarios in the Lower Bilate Catchment, Ethiopia. *Natural Hazards,* 118, 2199-2226. https://doi.org/10.1007/s11069-023-06101-y.

Emrouznejad, A. & Ho, W. (2018) Fuzzy analytic hierarchy process. Boca Raton, Florida. CRC Press.

Gigovic', L., Pamučar, D., Bajic', Z. & Drobnjak, S. (2017) Application of GIS-interval rough AHP methodology for flood mapping in urban areas. *Water,* 9 (360), 1-26. https://doi.org/10.3390/w9060360.

Hagos, Y.G., Andualem, T.G., Yibeltal, M. & Mengie, M.A. (2022) Flood hazard assessment and mapping using GIS integrated with multi-criteria decision analysis in Upper Awash River Basin, Ethiopia. *Applied Water Science,* 12 (148), 1-18. https://doi.org/10.1007/s13201-022-01674-8.

Hategekimana, Y., Yu, L., Nie, Y., Zhu, J., Liu, F. & Guo F. (2018) Integration of multi-parametric fuzzy analytic hierarchy process and GIS along the UNESCO world heritage: A flood hazard index, Mombasa Country, Kenya. *Natural Hazards,* 92 (2), 1137-1153. https://doi.org/10.1007/s11069-018-3244-9.

Hu, S., Cheng, X., Zhou, D. & Zhang, H. (2017) GIS-based flood risk assessment in suburban areas: A case study of the Fangshan District, Beijing. *Natural Hazards,* 87, 1525-1543. https://doi.org/10.1007/s11069-017-2828-0.

Hussain, M., Tayyab, M., Zhang, J., Shah, A.A., Ullah, K., Mehmood, U. & Al-Shaibah, B. (2021) GIS-based multi-criteria approach for flood vulnerability assessment and mapping in District Shangla: Khyber Pakhtunkhwa, Pakistan. *Sustainability,* 13 (3126), 1-29. https://doi.org/10.3390/su13063126.

Lai, C., Chen, X., Chen, X., Wang, Z., Wu, X. & Zhao, S. (2015) A fuzzy comprehensive evaluation model for flood risk based on the combination weight of game theory. *Natural Hazards,* 77 (2), 1243-1259. http://dx.doi.org/10.1007/s11069-015-1645-6.

Li, C. & Fang, H. (2021) Assessment of climate change impacts on the streamflow for the Mun River in Mekong Basin, Southeast Asia: using SWAT model. *Catena,* 201, 1-13. http://dx.doi.org/10.1016/j.catena.2021.105199.

Liu, Y., Eckert, C.M. & Earl, C. (2020) A review of fuzzy AHP methods for decision making with subjective judgements. *Expert System with Applications,* 161 (113738), 1-30. https://doi.org/10.1016/j.eswa.2020.113738.

M′Barek, S., Rochdi, A., Bouslihim, Y. & Miftan A. (2021) Multi-site calibration and validation of SWAT model for hydrologic modeling and soil erosion estimation: A case study in El Grou Watershed, Morocco. *Ecological Engineering and Environmental Technology,* 22 (6), 45-52. http://dx.doi.org/10.12912/27197050/141593.

Maranzoni, A., D'Oria, M. & Rizzo, C. (2023) Quantitative flood hazard assessment methods: a review. *Journal of Flood Risk Management,* 16 (1), 1-31. https://doi.org/10.1111/jfr3.12855.

Nut, N. & Plermkamon, V. (2013) Estimation of flood damages on Nam Phong River by HEC-RAS. In: The 6th International Conference, SWE-04, 179-86.

Parhi, P.K., Sankhua, R.N. & Roy, G.P. (2012) Calibration of channel roughness for Mahanadi River, (India) using HEC-RAS model. *Journal of Water Resource and Protection,* 4 (10), 847-850. http://dx.doi.org/10.4236/jwarp.2012.410098.

Parsian, S., Amani, M., Moghimi, A., Ghorbanian, A. & Mahdavi, S. (2021) Flood hazard mapping using fuzzy logic, analytical hierarchy process, and multi-source geospatial datasets. *Remote Sensing,* 13 (23), 4761-4783. https://doi.org/10.3390/rs13234761.

Pawattana, C., Panasoontorn, S., Poopiwkham, S. & Ikhwali, F. (2021) Assessment of water shortage situations in Lower Nam Pong Basin under climate change. *Naresuan University Journal: Science and Technology,* 29 (4), 52-6. https://doi.org/10.14456/nujst.2021.35.

Peng, G., Han, L., Liu, Z., Guo, Y., Yan, J. & Jia, X. (2021) An application of fuzzy analytic hierarchy process in risk evaluation model. *Frontiers in Psychology,* 12, 1-12. https://doi.org/10.3389/fpsyg.2021.715003.

Poopiwkham, S. (2018) Development of potential flood maps using fuzzy logic due to climate change in Pong River Basin [Thesis]. Department of Civil Engineering: Khon Kaen University.

Promchote, P., Wang S.Y.S., & Johnson, P.G. (2016) The 2011 great flood in Thailand: Climate diagnostics and implications from climate change. *Journal of Climate,* 29 (1), 367-79.

Putra, M.S.D., Andryana, S., Fauziah, K. & Gunaryati, A. (2018) Fuzzy analytical hierarchy process method to determine the quality of gemstones. *Advance in Fuzzy System,* 2018, 1-6. https://doi.org/10.1155/2018/9094380.

Satriagasa, C., Tongdeenok, P. & Kaewjampa, N. (2023) Assessing the implication of climate change to forecast future flood using SWAT and HEC-RAS model under CMIP5 climate projection in Upper Nan Watershed, Thailand. Sustainability. 15(5276), 1-21. https://doi.org/10.3390/su15065276.

Singkran, N. (2017) Flood risk management in Thailand: Shifting from a passive to a progressive paradigm. *International Journal of Disaster Risk Reduction,* 25, 92-100.

Swagatika, S., Paul, J.C., Sahu, A.P., Das, D.M. & Patra, A.K. (2022) Streamflow Simulation of Brahmani River Basin using SWAT model. *Biological Forum,* 14 (3), 1707-1714.

Vojinovic, Z., Hammond, M., Golub, D., Hirunsalee, S., Weesakul, S., Meesuk, V., Medina, N., Sanchez, A., Kumara, S. & Abbott, M. (2016) Holistic approach to flood risk assessment in areas with cultural heritage: A practical application in Ayutthaya, Thailand. *Natural Hazards,* 81, 589-616. https://doi.org/10.1007/s11069-015-2098-7.

Yang, X., Ding, J. & Hou, H. (2013) Application of a triangular fuzzy AHP approach for flood risk evaluation and response measures analysis. *Natural Hazards.,* 68, 657-674. http://dx.doi.org/10.1007/s11069-013-0642-x.

Yodying, A., Mahavik, N., Tantanee, S., Kongmuang, C., Keteku, A.K., Chidburee P, Seejata, K. & Chatsudarat, S. (2022) A fuzzy AHP approach to assess flood hazard for area of Bang Rakam model 60 project in Yom River Basin, Northern Thailand. *Applied Environmental Research,* 44 (1), 108-125. https://doi.org/10.35762/AER.2021.44.1.9.